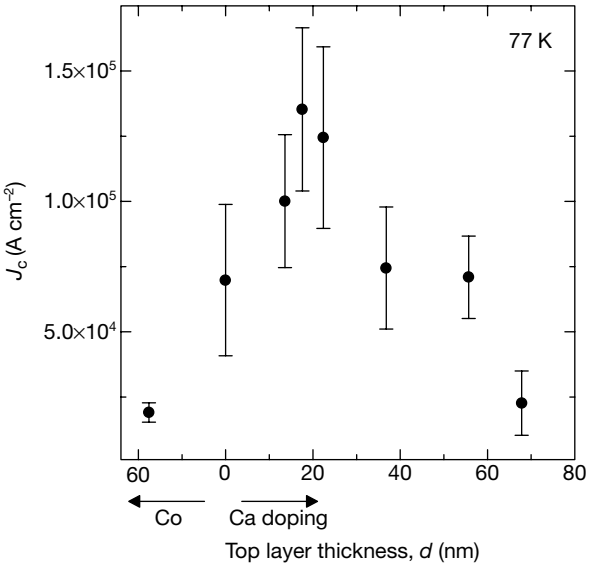

Figure 4 Dependence of the grain boundary critical current density J_c on the thickness of the doped top layer in doping bilayers. The figure shows the critical current density of 24° symmetric [001] tilt grain boundaries in doping bilayers about 160 nm thick at 77 K, plotted as a function of the thickness d of the doping top layer. On the right side of the figure, the data from $YBa_2Cu_3O_{7-\delta}/Y_{0.7}Ca_{0.3}Ba_2Cu_3O_{7-\delta}$ bilayers are plotted. On the left side the data from $YBa_2Cu_3O_{7-\delta}/YBa_2Cu_{2.9}Co_{0.1}O_{7-\delta}$ bilayers are shown. For the Co-doped samples the scale of the x-axis is compressed by a factor of three.

Fig. 1a, achieve critical current densities of 1.6×10^5 A cm^{-2} at 77 K for $x = 0.1$, $d = 25$ nm, and a periodicity of 50 nm.

For several samples, the dependence of the critical current on the applied magnetic field H, oriented parallel to the c-direction of the films, was measured. The maximum fields applied were 250 μT. All samples showed the $I_c(H)$ dependencies expected for 24° grain-boundary Josephson junctions.

For the large-scale fabrication of coated-conductor-based superconducting cables, techniques such as ion beam assisted deposition (IBAD)[11–13] or the rolling assisted biaxially aligned substrate process (RABITS)[14] are being developed in order to enhance J_c by providing an optimal alignment of the grains[2,3]. It is extremely desirable to lessen the required accuracy of the grain alignment. The use of doping heterostructures, which can easily be incorporated into these processes, may achieve this goal, as it presents a way of extending the established grain-boundary-angle-dependent limits on the critical current densities at 77 K (refs 2, 3). We anticipate that this will indeed be the case, considering that interface-charging and band-bending play an important role for small-angle grain boundaries as well[8,9]. □

Received 21 March; accepted 16 August 2000.

1. Bednorz, J. G. & Müller, K. A. Possible high T_c superconductivity in the Ba-La-Cu-O system. *Z. Phys. B* **64,** 189–193 (1986).
2. Dimos, D., Chaudhari, P. & Mannhart, J. Superconducting transport properties of grain boundaries in $YBa_2Cu_3O_7$ bicrystals. *Phys. Rev. B* **41,** 4038–4049 (1990).
3. Ivanov, Z. G. *et al.* Weak links and dc SQUIDs on artificial nonsymmetric grain boundaries in $YBa_2Cu_3O_{7-\delta}$. *Appl. Phys. Lett.* **59,** 3030–3032 (1991).
4. Heinig, N. F., Redwing, R. D., Nordman, J. E. & Larbalestier, D. C. Strong to weak coupling transition in low misorientation angle thin film $YBa_2Cu_3O_{7-\delta}$ bicrystals. *Phys. Rev. B* **60,** 1409–1417 (1999).
5. Mannhart, J. & Hilgenkamp, H. Wavefunction symmetry and its influence on superconducting devices. *Supercond. Sci. Technol.* **10,** 880–883 (1997).
6. Mannhart, J. & Hilgenkamp, H. Possible influence of band bending on the normal state properties of grain boundaries in high-T_c superconductors. *Mater. Sci. Eng. B* **56,** 77–85 (1998).
7. Hilgenkamp, H. & Mannhart, J. Superconducting and normal-state properties of $YBa_2Cu_3O_{7-\delta}$-bicrystal grain boundary junctions in thin films. *Appl. Phys. Lett.* **73,** 265–267 (1998).
8. Gurevich, A. & Pashitskii, E. A. Current transport through low-angle grain boundaries in high-temperature superconductors. *Phys. Rev. B* **57,** 13878–13893 (1998).
9. Schmehl, A. *et al.* Doping-induced enhancement of the critical currents of grain boundaries in $YBa_2Cu_3O_{7-\delta}$. *Europhys. Lett.* **47,** 110–115 (1999).
10. Ivanov, Z. G., Stepantsov, E. A., Tzalenchuk, A. Y. & Claeson, T. Properties of locally doped bi-crystal grain boundary junctions. *Physica B* **194–196,** 2187–2188 (1994).
11. Iijima, Y., Tanabe, N., Kohno, O. & Ikeno, Y. In-plane aligned $YBa_2Cu_3O_{7-x}$ thin films deposited on polycrystalline metallic substrates. *Appl. Phys. Lett.* **60,** 769–771 (1992).
12. Reade, R. P., Berdahl, P., Russo, R. E. & Garrison, S. M. Laser deposition of biaxially textured yttria-stabilized zirconia buffer layers on polycrystalline metallic alloys for high critical current Y-Ba-Cu-O thin films. *Appl. Phys. Lett.* **61,** 2231–2233 (1992).
13. Wu, X. D. *et al.* Properties of $YBa_2Cu_3O_{7-\delta}$ thick films on flexible buffered metallic substrates. *Appl. Phys. Lett.* **67,** 2397–2399 (1995).
14. Norton, D. P. *et al.* Epitaxial $YBa_2Cu_3O_7$ on biaxially textured nickel (001): an approach to superconducting tapes with high critical current density. *Science* **274,** 755–757 (1996).

Acknowledgements

We are grateful for valuable discussions with D. G. Schlom. This work was supported by the Bundesministerium für Bildung und Forschung. H.H. thanks the Royal Dutch Academy of Sciences for its support.

Correspondence and requests for materials should be addressed to J.M. (e-mail: jochen.mannhart@physik.uni-augsburg.de).

Thin films of fullerene-like MoS_2 nanoparticles with ultra-low friction and wear

Manish Chhowalla & Gehan A. J. Amaratunga

Engineering Department, University of Cambridge, Trumpington Street, Cambridge CB2 1PZ, UK

The tribological properties of solid lubricants such as graphite and the metal dichalcogenides MX_2 (where M is molybdenum or tungsten and X is sulphur or selenium)[1–13] are of technological interest for reducing wear in circumstances where liquid lubricants are impractical, such as in space technology, ultra-high vacuum or automotive transport. These materials are characterized by weak interatomic interactions (van der Waals forces) between their layered structures, allowing easy, low-strength shearing[14,15]. Although these materials exhibit excellent friction and wear resistance and extended lifetime in vacuum, their tribological properties remain poor in the presence of humidity or oxygen[16–19], thereby limiting their technological applications in the Earth's atmosphere. But using MX_2 in the form of isolated inorganic fullerene-like hollow nanoparticles similar to carbon fullerenes and nanotubes can improve its performance[1]. Here we show that thin films of hollow MoS_2 nanoparticles, deposited by a localized high-pressure arc discharge method, exhibit ultra-low friction (an order of magnitude lower than for sputtered MoS_2 thin films) and wear in nitrogen and 45% humidity. We attribute this 'dry' behaviour in humid environments to the presence of curved S–Mo–S planes that prevent oxidation and preserve the layered structure.

Thus far, only isolated MoS_2 and WS_2 nanoparticles have been generated by solid–gas reaction or electron-beam irradiation[20,21]. Here we report the friction and wear properties of thin films of MoS_2 nanoparticles, deposited using a localized high-pressure arc discharge[22,23] (see Methods section). Films deposited by arc discharge, but in the absence of localized high pressure, appear mostly amorphous with only local hexagonal structure when studied by high-resolution electron microscopy (HREM). However, circular nanoparticles (Fig. 1a) and curved S–Mo–S planes (Fig. 1b) are readily seen for films deposited by arc discharge in the presence of high-pressure nitrogen. The key mechanism in the formation of nanoparticles is the bending and rearrangement of the basal planes[24]. Displacement of Mo or S via collisions with energetic

ions in the arc plasma[25] can lead to rearrangement of atoms in order to maintain electrical neutrality. The results shown in Fig. 1 indicate that it is possible to generate well formed hollow fullerene-like 'onion' MoS_2 clusters in the form of a thin film using the localized arc discharge method.

In addition to HREM, further information regarding the chemical composition and structure was obtained from X-ray diffraction (XRD) analysis. The XRD pattern of the nanoparticle MoS_2 film is shown in Fig. 2. A sharp (0002) peak is observed, along with peaks from other reflection groups. The (0002) peak in the XRD spectrum of the nanoparticle film is characterized by a shift to a lower angle as compared to the (0002) peak in hexagonal (2H) MoS_2 crystals. This shift in the (0002) peak indicates lattice expansion, and has been attributed to the introduction of strain owing to curvature of the layers[24]. In contrast, the (0002) peak shift in dense, oriented ion beam assisted deposition (IBAD). MoS_2 films has been attributed to straining of the basal plane spacing due to defects[26]. In lamellar lattices, the (000*l*) reflections are associated with ordering along the *c*-axis while the (*hk*0) reflections indicate ordering in the basal planes. The prominence of the (0002) peak in the XRD pattern of the nanoparticle MoS_2 film in Fig. 2 indicates the presence of well-stacked layered structure. An estimation of the grain size from the full-width at half-maximum of the (0002) reflection yields about 30 nm, in agreement with the average diameter of the nanoparticles observed in HREM. In Fig. 2, we have also plotted for comparison the XRD spectra from MoS_2 films produced by vacuum arc and d.c. sputtering techniques.

The friction coefficient (μ) and wear rate (w) of the films of MoS_2 nanoparticles were determined by the ball-on-disk (pure sliding) method[11,27]. The disks were the same ones used to measure the hardness and adhesion (see Methods). The results from the different types of films tested in our laboratory are summarized in Table 1. The evolution of μ as a function of the number of rubbings is plotted in Fig. 3. The nanoparticle MoS_2 films show a very low friction coefficient in a dry nitrogen atmosphere ($\mu = 0.006$). But our central result is that μ and w remain ultra-low even in 45% relative humidity in ambient conditions. In fact, μ and w are slightly lower for the nanoparticle MoS_2 film in 45% humidity than for the sputtered MoS_2 film in dry nitrogen.

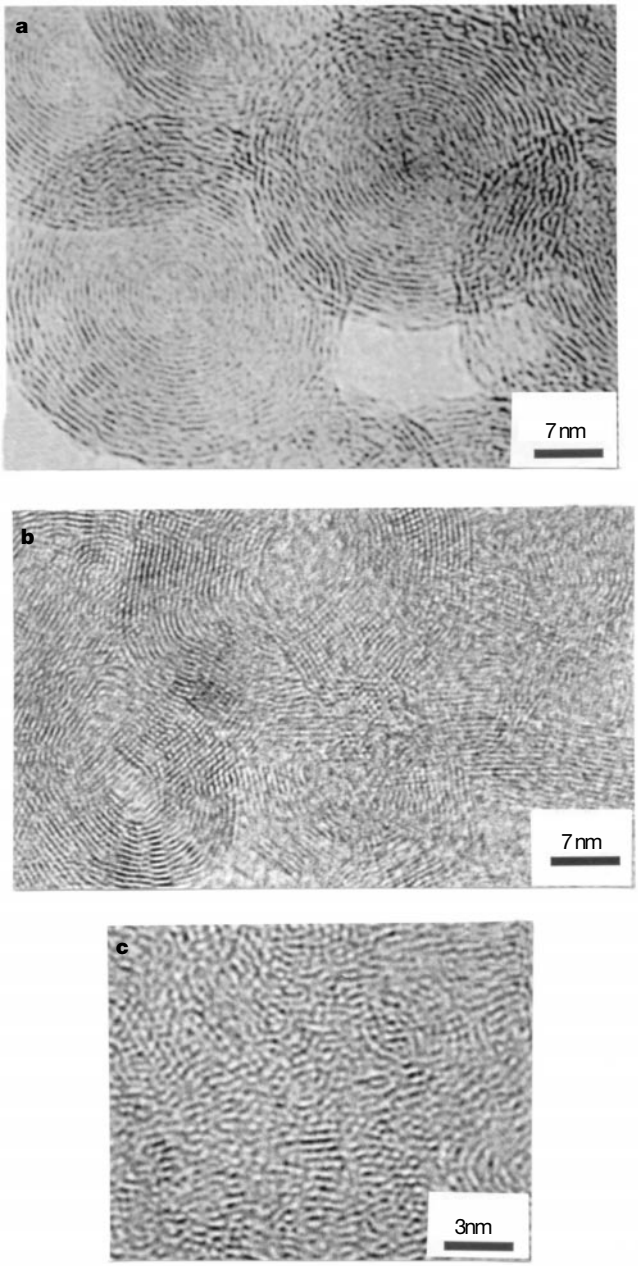

Figure 1 High-resolution transmission electron microscopy (TEM) images of 50-nm-thick films of MoS_2 nanoparticles. The films were deposited on Si[100] substrates, and the images were obtained using a JEOL 2000FX TEM operated at 200 kV. The TEM samples were prepared by dissolving the Si substrate in $HF:HNO_3:H_2O$ solution (or in water for NaCl substrates), and placing the freed fragments of the film onto Cu grids. Circular nanoparticles with diameters up to 30 nm are readily visible in **a**. Curved S–Mo–S planes forming irregularly shaped nanoparticles are shown in **b**. An image of a sputtered MoS_2 film is also shown in **c**, for comparison.

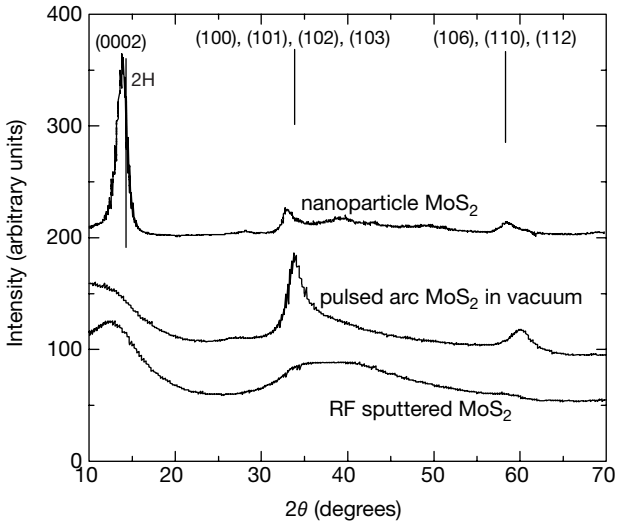

Figure 2 X-ray diffraction (XRD) patterns from thin films of MoS_2 nanoparticles. The figure shows results for three films: one produced by a localized high-pressure discharge, one deposited in vacuum, and one deposited by sputtering. The XRD was performed, using a Siemens MRD diffractometer with a Cu source, on 1.2-μm-thick films deposited on 440C stainless steel disks. In order to enhance the signal from the thin films, all measurements were performed at a grazing angle of $\alpha = 3°$. XRD spectra obtained from films deposited on background-free quartz also revealed a similar pattern. The nanoparticle MoS_2 film shows a sharp (0002) peak, in contrast to the vacuum-arc and sputter-deposited films in which other reflections dominate the XRD pattern. The slight shift of the (0002) peak indicated by the vertical line is explained in the text.

Table 1 Results of tribological tests on MoS_2 films

Film	μ	w ($mm^3 N^{-1} mm^{-1}$)
Nanoparticle MoS_2	0.008–0.01	$\sim 1 \times 10^{-11}$
Sputtered MoS_2	0.1–0.3	$\sim 3 \times 10^{-9}$
Hard TiN	0.4–0.6	NA

μ is measured friction coefficient in 45% relative humidity in ambient conditions; w is the wear rate. NA, not available.

Examinations of the wear patterns (Fig. 3b,c) on the uncoated ball show clear differences between the nanoparticle and the sputtered films. In the sputtered film, a heavily worn and rough surface with bright and shiny wear tracks along with some dark patches can be seen (Fig. 3c). The wear pattern on the uncoated ball after failure was also examined under a scanning electron microscope fitted with energy dispersive X-ray (EDX) detector. EDX analysis revealed predominantly iron oxide in the wear scar. X-ray photoelectron spectroscopy (XPS) analysis of the wear region on the coated disk also confirmed the formation of MoO_3 on the sputtered film (after failure). The test on the nanoparticle film was stopped before failure after 2.4×10^5 rubbings (three times longer than the rubbings to failure in the sputtered film) owing to the limitations of our experimental apparatus. In contrast to Fig. 3c, substantial wear in the form of bright and dark patches was not observed in the scar of the ball mating with the nanoparticle MoS_2 film (Fig. 3b). Instead, substantial film transfer from the coated disk to the uncoated ball can be seen. EDX analysis of the worn region in Fig. 3b showed that primarily molybdenum and sulphur were present, with only residual peaks arising from carbon and oxygen. The XPS analysis of the worn region on the nanoparticle MoS_2 film before failure revealed a smaller MoO_3 peak than the sputtered film.

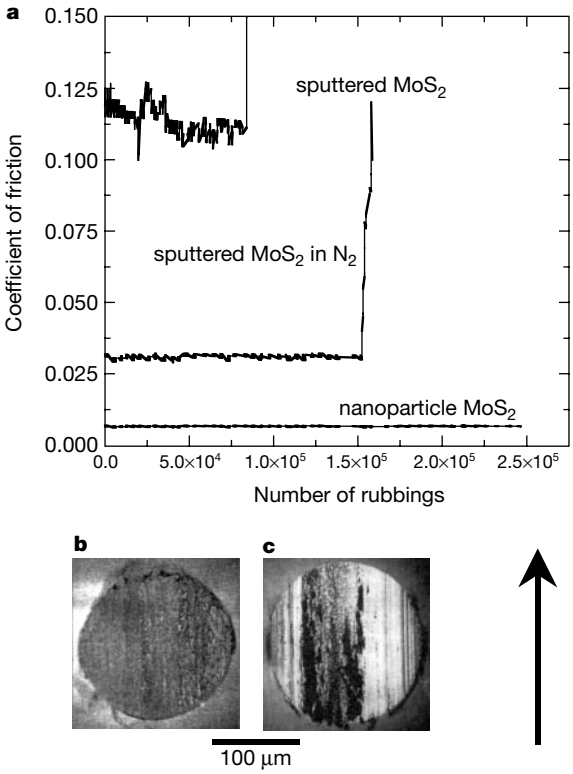

Figure 3 Wear tests on MoS_2 films in different atmospheres. **a**, The coefficient of friction as a function of time for: sputtered MoS_2 films in 45% relative humidity in ambient conditions (top curve); sputtered MoS_2 films in dry nitrogen; and nanoparticle MoS_2 films in 45% humidity formed by the procedure described in this work. Note that each curve is an average of ten different measurements on at least three different samples. The friction coefficient was obtained by a unidirectional 'ball on flat disk' (pure sliding) wear test (see Methods). The mating ball was also made from 440C stainless steel with a diameter of 0.7 cm and of comparable average roughness to the disk. The applied load was 10 N (using a dead-weight) on to the rotating disk (speed, 50 cm s^{-1}) which gave a maximum hertzian pressure of ~1.1 GPa and contact diameter of ~100 μm. Calibration of the ball-on-disk was performed to ensure that the tilt of the disk was within 0.5°, which gave a tolerance of ±0.009 for the friction coefficient. The mating ball was uncoated. The wear rate for the disk was obtained by determining the cross-sectional area of the wear track. The wear patterns for nanoparticle (**b**) and sputtered (**c**) MoS_2 films were obtained using a light optical microscope. The arrow indicates the direction of sliding.

In order to study the structural changes in the film after the test, MoS_2 debris from the wear scar of the nanoparticle film was observed under HREM. The observations revealed that although the curved hexagonal lattice is still maintained (Fig. 4), almost no closed circular nanoparticles remained, indicating that under these loading conditions the large fullerenes fragment into smaller irregularly shaped closed crystallites. An HREM image of the nanoparticle film after 2.4×10^5 rubbings is shown in Fig. 4.

Although the tribological properties of MoS_2 powder and MoS_2 thin films have been investigated for decades, the mechanisms responsible for the lubrication process remain unclear[4,6–9,11]. The combination of factors such as maintenance of the lamellar structure, formation and adhesion of a homogeneous transfer film, prevention of oxidation and intercrystallite slip have been cited as possible mechanisms responsible for the successful performance of MoS_2 as a solid boundary lubricant[4–11]. In the case of WS_2 nanoparticles dispersed in oil, rolling friction along with the absence of dangling bonds may be responsible for the low μ and w (ref. 1). In contrast, we believe that the mechanisms responsible for the low friction coefficient in fullerene-like MoS_2 films are probably similar to sputtered films but with additional features. The tribological properties of sputtered MoS_2 films are correlated to its microstructure, and the variations are attributed to differences in deposition parameters or the degree of water vapour present during processing[11]. Annealing of sputtered MoS_2 films can lead to the sharpening of the (0002) XRD peak, as well as the appearance of short, two-dimensional hexagonal crystals in HREM which in turn has been correlated to the decrease in the friction coefficient[28]. Therefore, it is feasible that highly ordered and pure MoS_2 could have an intrinsically low friction coefficient if the low-shear-strength properties are maintained during tribological testing. In our case, the coating process was initiated at a base pressure of 1×10^{-5} Pa and the substrates were held at 200 °C, so contamination during deposition is insignificant. The HREM images (Fig. 1a, b) primarily show circular nanoparticles and curved S–Mo–S planes, along with fine amorphous regions, before testing. Furthermore, the XRD shows strong ordering in the *c*-axis.

Taking into account the HREM, XRD, EDX and XPS data, our results clearly indicate that it is possible to improve the friction and wear properties of MoS_2 thin films by the incorporation of fullerene-like nanoparticles. We argue that the low friction coefficient measured for the nanoparticle films may simply be a consequence of the highly ordered curved structure. That is, the incorporation of nanoparticles through localized high-pressure arc discharge allows the deposition of a highly ordered MoS_2 structure that is not (or may not be) accessible by sputtering or other methods[29]. Further-

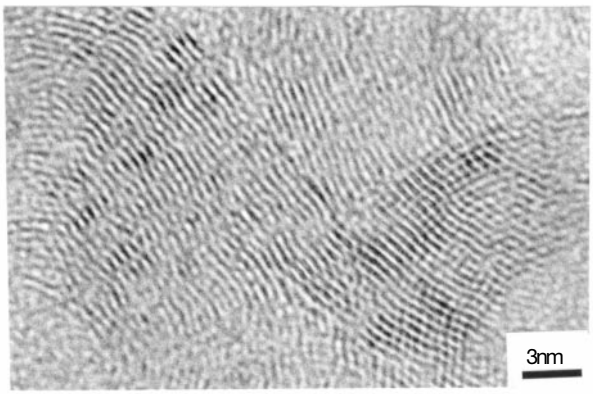

Figure 4 HREM image of debris collected from the wear track region of an MoS_2 nanoparticle film after the reciprocating wear test in 45% relative humidity in ambient conditions. The image clearly shows the presence of curved hexagonal planes.

more, mechanisms such as intercrystallite slip can still occur in fragmented nanoparticles and crystallites consisting of irregularly shaped curved S–Mo–S planes, even though shearing between the layers is unlikely in closed nanoparticles. An additional feature of these films is the presence of curved hexagonal planes that clearly enhance the stability of the material in humid environments, and thus help to preserve the lamellar structure longer. In the case of MoS_2 powder (or sputtered film), oxidation can occur through unterminated bonds of the hexagonal planes, causing the material to stick, leading to rapid deterioration of its low-shear-strength properties. The curvature of the hexagonal planes appears to buffer the Mo atom from oxidation by reducing the number of exposed dangling bonds at the edges of the planes.

The deposition of films of MoS_2 nanoparticles could be easily incorporated into existing thin-film technology for coating automotive parts and tool components. The deposition method that we report here allows the formation of the low-friction layer directly onto the components instead of dispersing the nanoparticles into oil, which could lead to adverse clogging. The low-temperature nature of the process also allows it to be used on top of hard, or magnetic, thin films to give a low-friction layer. Finally, we note that the ultra-low friction coefficients measured here may point towards the intrinsic tribological properties of highly ordered solid MoS_2, but additional fundamental study is required to test this hypothesis. □

Methods

Deposition of nanoparticle MoS_2

The nanoparticle MoS_2 films were deposited by ablating a solid MoS_2 target by an arc discharge in the presence of localized high-pressure nitrogen, similar to the technique used to generate thin films of nanoparticle carbon[22,23]. The localized high pressure is generated by introducing the carrier gas via a 1-mm hole in the MoS_2 target. The dynamics involved in the formation of MoS_2 nanoparticles are at present unclear but the mechanism is probably similar to the formation of carbon nanoparticles, as the technique used here is identical and is described in detail elsewhere[22,23]. The nanoparticles of MoS_2 are thought to form immediately above the cathode surface, and to be carried via expansion from the localized high-pressure region near the arc discharge to the substrate; the substrate is placed 20 cm away, where the pressure is kept constant at 10 mtorr (refs 22,23). The films were deposited at 200 °C. The arc was ignited (at 75 A and ~22 V) in the localized region of high-pressure nitrogen.

Mechanical properties of nanoparticle MoS_2

The films were deposited on disks of 440C stainless steel; these disks were 5 cm in diameter, 0.8 cm thick, and were used for all the mechanical and tribological measurements reported here. The substrates were lap-polished so that the final average roughness value was 0.04–0.05 μm. The film thickness was kept constant at 1.2 ± 0.1 μm for all the mechanical and tribological tests. The adhesion, measured using a VTT scratch tester with a 200-μm Rockwell C indenter and maximum load of 100 N with a load rate of 1.7 N s^{-1}, was found to be 25 N. The hardness of the films was measured using a Fisher microindentation system with Berkovich (pyramidal) tip[22]. The hardness, extracted using the plastic displacement obtained from the intercept with the displacement axis of the unloading curve at maximum applied load (5 mN), was found to be 10 GPa, comparable to values reported for sputtered MoS_2 (ref. 30). The surface roughness of the deposited film measured using the Dektak IIA profilometer was found to be approximately 30 nm.

Received 25 October 1999; accepted 20 June 2000.

1. Rapoport, L. *et al.* Hollow nanoparticles of WS_2 as potential solid-state lubricants. *Nature* **387,** 791–793 (1997).
2. Bell, M. E. & Findlay, J. H. Molydenite as a new lubricant. *Phys. Rev.* **59,** 922–927 (1941).
3. Braithwaite, E. R. & Rowe, G. W. Principles and applications of lubrication with solids. *Sci. Lubricat.* **15,** 92–96 (1957).
4. Winer, W. O. Molybdenum disulphide as a lubricant: A review of the fundamental knowledge. *Wear* **10,** 422–452 (1967).
5. Spalvins, T. Lubrication with sputtered MoS_2 films. *ASLE Trans.* **14,** 267–271 (1972); Morphological and frictional behavior of sputtered MoS_2 films. *Thin Solid Films* **96,** 17–24 (1982).
6. Holinski, R. & Gansheimer, J. A study of the lubricating mechanism of molybdenum disulphide. *Wear* **19,** 329–342 (1972).
7. Buck, V. Morphological properties of sputtered MoS_2 films. *Wear* **91,** 281–288 (1983).
8. Fleischauer, P. D. & Tolentino, L. U. Effects of crystallite orientation on the environmental stability and lubrication properties of sputtered MoS_2 thin films. *ASLE Trans.* **27,** 82–88 (1984).
9. Roberts, E. W. Thin solid lubricants in space. *Tribol. Int.* **23,** 95–104 (1990).
10. Miyoshi, K. *et al.* A vacuum (10^{-9} Torr) friction apparatus for determining friction and endurance like that of MoS_x films. *Tribol. Trans.* **36,** 351–358 (1993).
11. Suzuki, M. Comparison of tribological characteristics of sputtered MoS_2 films coated with different apparatus. *Wear* **218,** 110–118 (1998).
12. Wang, D. Y., Chang, C. L., Chen, Z. Y. & Ho, W. Y. Microstructural characterization of MoS_2-Ti composite solid lubricating films. *Surf. Coat. Technol.* **121,** 629–635 (1999).
13. Killeffer, D. H. & Linz, D. *Molybdenum Compounds: Their Chemistry and Technology* (Interscience, New York, 1952).
14. Dickinson, R. G. & Pauling, L. The crystal structure of molybdenite. *J. Am. Chem. Soc.* **45,** 1466–1471 (1923).
15. Bragg, W. The investigation of the properties of thin films by means of x-rays. *Nature* **115,** 266–269 (1925).
16. Williams, J. A. *Engineering Tribology* 368–370 (Oxford Univ. Press, 1994).
17. Savage, R. H. Graphite lubrication. *J. Appl. Phys.* **19,** 1–10 (1948).
18. Arnell, R. D., Davies, P. B., Halling, J. & Whomes, T. L. *Tribology—Principles and Design Applications* 105–107 (Macmillan, London, 1991).
19. Matsumoto, K. & Suzuki, M. in *Proc. Int. Tribology Conf. 1995* 1165–1169 (JST, Tokyo, 1996).
20. Feldman, Y., Wasserman, E., Srolovitz, D. J. & Tenne, R. High-rate, gas-phase growth of MoS_2 nested inorganic fullerenes and nanotubes. *Science* **267,** 222–225 (1995).
21. Jose-Yacaman, M. *et al.* Studies of MoS_2 structures produced by electron irradiation. *Appl. Phys. Lett.* **69,** 1065–1067 (1996).
22. Amaratunga, G. A. J. *et al.* Hard elastic carbon thin films from linking of carbon nanoparticles. *Nature* **383,** 321–323 (1996).
23. Chhowalla, M., Aharanov, R. A., Kiely, C. J., Alexandrou, I. A. & Amaratunga, G. A. J. Generation and deposition of fullerene- and nanotube-rich carbon thin films. *Phil. Mag. Lett.* **75,** 329–335 (1997).
24. Srolovitz, D. J., Safran, S. A., Homyonfer, M. & Tenne, R. Morphology of nested fullerenes. *Phys. Rev. Lett.* **74,** 1779–1782 (1995).
25. Bilek, M. M. M., Martin, P. J. & McKenzie, D. R. Influence of gas pressure and cathode composition on ion energy distributions in filtered vacuum arcs. *J. Appl. Phys.* **83,** 2965–2970 (1998).
26. Dunn, D. N., Seitzman, L. E. & Singer, I. L. The origin of anomalous low (0002) peak in x-ray diffraction spectra of MoS_2 films grown by ion beam assisted deposition (IBAD). *J. Mater. Res.* **12,** 1191–1194 (1997).
27. Westergard, R. & Axén, N. *Tribologia—Finn. J. Tribol.* **17,** 14–18 (1998).
28. Mattern, N., Hermann, H., Weise, G., Teresiak, A. & Bauer, H. D. Structure and properties of MoS_2 films. *Mater. Sci. Forum* **235–238,** 613–618 (1997).
29. Dunn, D. N., Seitzman, L. E. & Singer, I. L. MoS_2 deposited by ion beam assisted deposition: 2H or random layer structure? *J. Mater. Res.* **13,** 3001–3007 (1998).
30. Fox, V. C., Renevier, N., Teer, D. G., Hampshire, J. & Rigato, V. The structure of tribologically improved MoS_2-metal composite coatings and their industrial applications. *Surf. Coat. Technol.* **119,** 492–497 (1999).

Acknowledgements

We thank R. Aharonov for general assistance and advice, and J. A. Williams for discussions.

Correspondence and requests for materials should be addressed to G.A.J.A. (e-mail: ga@eng.cam.ac.uk).

Helical self-assembled polymers from cooperative stacking of hydrogen-bonded pairs

J. H. K. Ky Hirschberg, Luc Brunsveld, Aissa Ramzi, Jef A. J. M. Vekemans, Rint P. Sijbesma & E. W. Meijer

Laboratory of Macromolecular and Organic Chemistry and Dutch Polymer Institute, Eindhoven University of Technology, PO Box 513, 5600 MB Eindhoven, The Netherlands

The double helix of DNA epitomizes this molecule's ability to self-assemble in aqueous solutions into a complex chiral structure using hydrogen bonding and hydrophobic interactions. Non-covalently interacting molecules in organic solvents are used to design systems that similarly form controlled architectures[1–7]. Peripheral chiral centres in assemblies[8,9] and chiral side chains attached to a polymer backbone[10,11] have been shown to induce chirality at the supramolecular level, and highly ordered structures stable in water are also known[12–15]. However, it remains difficult to rationally exploit non-covalent interactions for the formation of chiral assemblies that are stable in water, where solvent molecules can compete effectively for hydrogen bonds. Here we describe a general strategy for the design of functionalized monomer units and their association in either water or alkanes into non-covalently linked polymeric structures with controlled helicity and chain length. The monomers consist of bifunctionalized ureidotriazine units connected by a spacer and